

Lawrence Berkeley National Laboratory

Recent Work

Title

Charged Particle Method, Protons and Heavy Charged Particles

Permalink

<https://escholarship.org/uc/item/4000g437>

Authors

Frankel, K.A.

Phillips, M.H.

Publication Date

1993



Lawrence Berkeley Laboratory

UNIVERSITY OF CALIFORNIA

To be published as a chapter in *Physical Aspects of Stereotactic Radiosurgery*, M.H. Phillips, Ed., Plenum Publishing, New York, NY, 1993

Charged Particle Method — Protons and Heavy Charged Particles

K.A. Frankel and M.H. Phillips

October 1992

Donner Laboratory

Biology & Medicine Division

REFERENCE COPY
Does Not Circulate
Bidg. 50 Library.
Copy 1

DISCLAIMER

This document was prepared as an account of work sponsored by the United States Government. Neither the United States Government nor any agency thereof, nor The Regents of the University of California, nor any of their employees, makes any warranty, express or implied, or assumes any legal liability or responsibility for the accuracy, completeness, or usefulness of any information, apparatus, product, or process disclosed, or represents that its use would not infringe privately owned rights. Reference herein to any specific commercial product, process, or service by its trade name, trademark, manufacturer, or otherwise, does not necessarily constitute or imply its endorsement, recommendation, or favoring by the United States Government or any agency thereof, or The Regents of the University of California. The views and opinions of authors expressed herein do not necessarily state or reflect those of the United States Government or any agency thereof or The Regents of the University of California and shall not be used for advertising or product endorsement purposes.

Lawrence Berkeley Laboratory is an equal opportunity employer.

DISCLAIMER

This document was prepared as an account of work sponsored by the United States Government. While this document is believed to contain correct information, neither the United States Government nor any agency thereof, nor the Regents of the University of California, nor any of their employees, makes any warranty, express or implied, or assumes any legal responsibility for the accuracy, completeness, or usefulness of any information, apparatus, product, or process disclosed, or represents that its use would not infringe privately owned rights. Reference herein to any specific commercial product, process, or service by its trade name, trademark, manufacturer, or otherwise, does not necessarily constitute or imply its endorsement, recommendation, or favoring by the United States Government or any agency thereof, or the Regents of the University of California. The views and opinions of authors expressed herein do not necessarily state or reflect those of the United States Government or any agency thereof or the Regents of the University of California.

LBL-34005
UC-408

**Charged Particle Method: Protons and
Heavy Charged Particles**

In M. H. Phillips (ed):
Physical Aspects of Stereotactic Radiosurgery
Plenum Publishing, New York, 1993

Kenneth A. Frankel, Ph.D.

Mark H. Phillips, Ph.D.

Life Sciences Division
Lawrence Berkeley Laboratory
University of California at Berkeley
Berkeley, CA 94720

May 1993

This research was supported by the Director, Office of Energy Research,
Office of Health and Environmental Research, Medical Applications Division
of the U.S. Department of Energy under Contract No. DE-AC03-76SF00098.

Chapter 2

CHARGED PARTICLE METHOD

Protons and Heavy Charged Particles

KENNETH A. FRANKEL, PH.D.

MARK H. PHILLIPS, PH.D.

2.1 Rationale and Background

Protons and other heavy charged particles, such as deuterons and helium ions, were the first radiations to be used on a regular basis for stereotactic radiosurgery of intracranial targets [19, 20, 44, 45]. Leksell, Larsson, and colleagues in Sweden [15, 21, 22, 39] extensively explored the effects of focal irradiation in the mammalian brain using narrow beams of protons. Lawrence, Tobias, Linfoot, et al [19, 20, 26, 44, 45] developed charged particle radiosurgery for a number of different medical conditions at the Donner Laboratory, Lawrence Berkeley Laboratory (LBL) at the University of California-Berkeley. This early work in the 1950's and 1960's presaged the current status of charged particles in radiosurgery. Charged particles were shown to be an effective means of producing small, tightly circumscribed

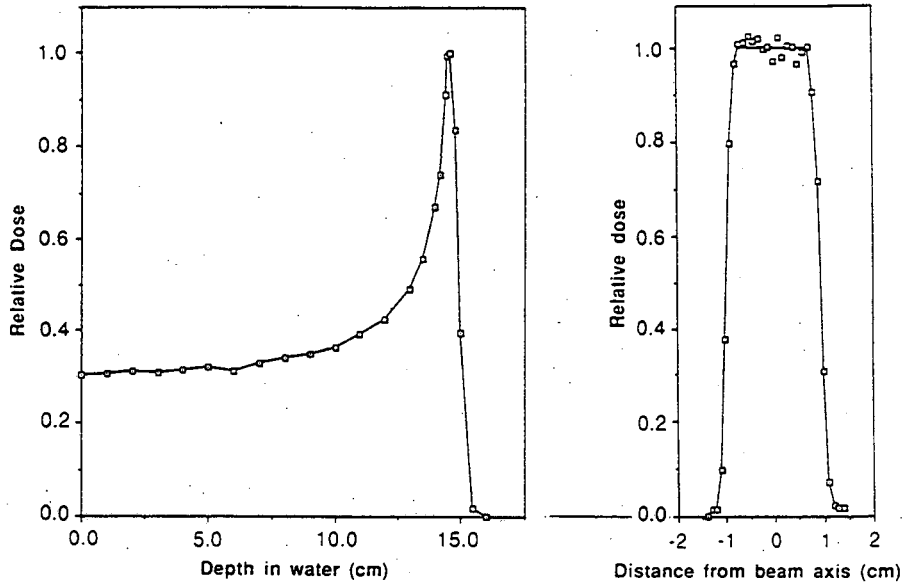


Figure 2.1: Measurements of the 165 MeV/amu helium ion beam at the LBL Bevatron. (Left) A Bragg curve measured as a function of depth in a water bath. The helium ion beam was collimated with a 2 cm collimator. (Right) The lateral dose profile in the water bath. This profile was measured 1 cm from the distal edge of a beam with a 7 cm residual range and with the Bragg peak spread 2 cm. The distal edge of the Bragg peak and the lateral sharpness are little affected by spreading the Bragg peak.

lesions in the brain with little or no damage to intervening or adjacent normal tissue. They exhibited unique advantages relative to photons in their ability to localize the dose and to avoid irradiation of critical brain structures. However, the complexity and expense of the hardware needed to produce them has slowed their integration into general medical practice.

The dose distribution of a beam of monoenergetic charged particles passing through a homogeneous medium, e.g. water, is characterized by a plateau region and the Bragg peak as illustrated in Fig. 2.1 [29]. The plateau is a region of relatively constant dose as a function of depth. In the directions perpendicular to the beam axis, the dose is constant across the beam with very steep fall-off

CHARGED PARTICLES

at the edges. The Bragg peak following the long plateau is a small region (approximately 1 to 5 mm long) of dose that is several times greater than in the plateau. The particles stop at the end of the Bragg peak region and there is virtually no dose distal to this point. As the particles approach the Bragg peak region, the lateral dose fall-off becomes less sharp.

By using a large number of beams that intersect at a common point in the plateau region of dose distribution, a very high dose gradient centered on that point can be achieved in all directions. A similarly steep gradient can be achieved with a much smaller number of beams that intersect at the Bragg peak. The plateau method has the advantage that exact calculations of the energy loss of the charged particles in the tissue necessary to properly place the Bragg peak are not needed. It suffices that the beam initially has enough energy to completely penetrate the head. It suffers from the disadvantage that tissues on the distal side of the target undergo irradiation, and more beamports are needed with a consequent increase in the volume of normal tissue irradiated. Conversely, the Bragg peak method requires more extensive calculations and calibrations, but minimizes the volume of normal tissue irradiated.

The extremely well-confined dose localization that is possible with beams of charged particles, with the possibility of delivering a therapeutic dose to the diseased tissue while sparing nearly all normal tissue from adverse consequences, led to the use of charged particles in radiosurgery in the 1950's. In Berkeley, over 1000 patients were treated for pituitary disorders using plateau proton, deuteron, and helium ion beams from the mid-1950's to the early 1970's [17, 18, 25, 26, 43]. In the early 1960's, treatments were begun at the Harvard Cyclotron Laboratory-Massachusetts General Hospital (HCL-MGH) using Bragg peak protons for the treatment of pituitary tumors and intracranial arteriovenous malformations [8, 9, 10, 11, 13, 14, 23]. In the 1960's, several proton accelerators in the Soviet Union were also brought into service for the treatment of pituitary tumors, conditions responsive to pituitary suppression, and AVMs. The treatments are performed using the plateau beam or the Bragg peak, depending on the size and type of lesion [23, 31, 32, 33, 34, 35]. In 1980, the treatment of AVMs was begun at the Lawrence Berkeley Labora-

tory (LBL) using the Bragg peak of helium ions [3, 4, 5, 24, 40]. In 1989, the protocol was enlarged to include the treatment of pituitary tumors that have recurred following surgical resection.

Although this chapter focusses on charged particles, it is appropriate to mention the one trial wherein neutral particles were used for radiosurgery. At the University of Washington, a 50 MeV cyclotron was used to deliver 9 Gy of fast neutron radiation for the treatment of inoperable arteriovenous malformations [7, 41, 42]. The radiation was delivered in 7 to 14 isocentric portals, each of which was shaped by a multi-leaf collimator. The depth-dose curve of 50 MeV neutrons is similar to 8 MV photons, so the dose distributions resemble photon dose distributions more than charged particle dose distributions. The use of a fixed number of shaped fields seems to be best tailored to treating larger lesions, and preliminary results are somewhat encouraging.

2.2 Physics of Charged Particles

2.2.1 Depth-Dose Characteristics

In this chapter, the phrase *charged particles* will refer to protons, deuterons, helium ions and heavier ions. Electrons and pions are excluded from this group. The differences in mass and stability between electrons and pions on the one hand, and the heavier charged particles on the other, change their dose deposition characteristics to such an extent that they are not comparable in the context of radiosurgical applications.

The deposition of dose by a charged particle as it passes through matter is characterized by: (a) the linear energy transfer (LET) to the traversed medium, (b) the particle range, and (c) scattering. The LET is the amount of energy deposited in the matter per unit distance travelled, and is a function of the composition of the material being traversed and the incident particle's charge and velocity.

$$LET = \frac{dE}{dx} \propto \frac{Z_{med}\rho_{med}}{A_{med}} \left(\frac{Z_{inc}}{v_{inc}} \right)^2 \quad (2.1)$$

where Z is the charge, A the atomic weight, ρ the density, and v the

CHARGED PARTICLES

velocity (*med* refers to the medium being traversed, and *inc* refers to the incident particle). This energy loss is due to collisions with electrons contained in the atoms and molecules of the material, and it is proportional to the electron density in the material. The collisions lead to a large number of electrons being ejected from the atoms and dissipating their energy in tracks emanating from the trajectory of the incident ion. The inverse proportionality of the LET to the incident particle velocity results in a very sharp increase in the energy deposited in the material as the velocity of the particle approaches zero, thereby giving rise to the Bragg peak.

The range of the particle is the distance the particle travels parallel to its incident direction. It is related to the LET by the equation:

$$\text{Range} = \int_E^0 \left(\frac{dE}{dx} \right)^{-1} dE \quad (2.2)$$

For a given incident energy and a given material, all charged particles of the same species will travel approximately the same distance. They will also deposit a large fraction of their energy in a region near the end of the range. Intuitively, one can picture the charged particles exchanging energy with the atoms of the target material as they speed by. As they interact with the nearby electrons, they give up some energy, and therefore they slow down. They spend more time in the vicinity of a given atom, give up even more energy, and slow down even more, and so on, until they come to an abrupt stop. Range straggling is the result of statistical fluctuations between different incident particles in the number and effect of the electron collisions that each undergoes. The range straggling, i.e. the dispersion of actual particle ranges about the mean range, is a Gaussian distribution with a typical width of 1-2% of the range.

Fig. 2.1 illustrates the measured Bragg peak of a 165 MeV/amu¹ helium ion beam at the Bevatron at LBL. The ratio of the energy deposited at the Bragg peak to that at the plateau is approximately 3:1. The range, as defined by the depth at which the dose falls to 90% of its peak dose, is 15 cm in water².

¹MeV = million electron volts, amu = atomic mass unit

²The exact range in the treatment room is dependent on the particular beam-

The heavier the particle, the more tightly is the dose confined to the Bragg peak. This characteristic was one of the reasons that helium ions were chosen for use at LBL rather than protons. Several reasons mitigate against using too heavy a particle. The first is that it requires more energy, and hence a more expensive accelerator, to accelerate a heavy particle to the energy needed to reach the same range as a lighter one. The second is that the biological effect is a function of the LET of a radiation, not just the dose. The ratio of the dose of a particular radiation to the dose of a standard x-radiation, e.g. 200 kVp photons, needed to produce a given biological effect is termed the relative biological effect (RBE) of that radiation. In the plateau region of light ions, such as protons and helium ions, the RBE is approximately 1. In the Bragg peak, where the LET is much higher, the RBE ranges from 1.0 to 1.3. For carbon and neon ions, the RBE can be much higher. The RBE values are dependent on the tissue and biological endpoint of interest, and these values are not well-known, especially in the brain. In addition, the type of biological damage may be qualitatively different for different LET radiations. Therefore, it is not a simple matter to use these high-LET radiations, and a measured approach is called for. Fragmentation of heavier ions, as described in 2.2.3, also results in increased dose distal to the target.

2.2.2 Lateral Scattering

In addition to collisions with electrons, the incident charged particles can also interact with the nuclei of the target material. The predominant nuclear interaction is between the charges (Coulomb fields) of the two particles. This leads to very little energy loss of the incident ion, but causes a deviation in the trajectory. The incident particle experiences many of these small scattering events as it passes through the medium. They all add up to form a Gaussian distribution about the incident direction, which is called the multiple Coulomb scattering distribution. It is this effect that leads to "unsharpness" of the beam in the directions perpendicular to the

line since energy losses occur in vacuum windows and beam monitoring devices.

CHARGED PARTICLES

incident direction. Multiple scattering increases as the particle energy decreases. Therefore, the width of the beam increases with the amount of material traversed; this effect is smaller for heavier ions. Fig. 2.2 demonstrates the effect of multiple scattering for beams of protons and helium ions. Both plots represent a beam of particles with an initial range of 15 cm in water that has been collimated with a 1 cm diameter collimator. As the charged particles penetrate the water, the tightly collimated beam spreads out. A comparison of the protons and the helium ions demonstrates that the heavier helium ions scatter significantly less for a given distance of penetration. High Z materials also produce a wider scattering distribution than low Z materials for the same energy loss of the incident ion.

2.2.3 Fragmentation

Charged particles can also undergo more radical nuclear interactions in which the incident charged particle or the target nucleus fragments. These fragments consist of protons, neutrons, and high Z ions, and are ejected from the collision with approximately the same energy and direction as the incident particle. These equal energy, but usually lighter, particles travel beyond the range of the incident particles, thereby contributing a dose beyond the distal edge of the primary beam. The cross-sections for fragmentation are strong functions of the incident particle species and the target species. For protons and helium, this phenomenon is of little consequence. It becomes noticeable with carbon ions and is an important factor with ions such as neon.

2.3 Beam Delivery

2.3.1 Charged Particle Accelerators

The particle accelerators used in all charged particle radiosurgical treatment programs were built originally for nuclear physics research. The 184" Synchrocyclotron at Berkeley was used for both purposes until the 1970's when the physics research moved to other accelerators, giving the medical research program sole possession. This

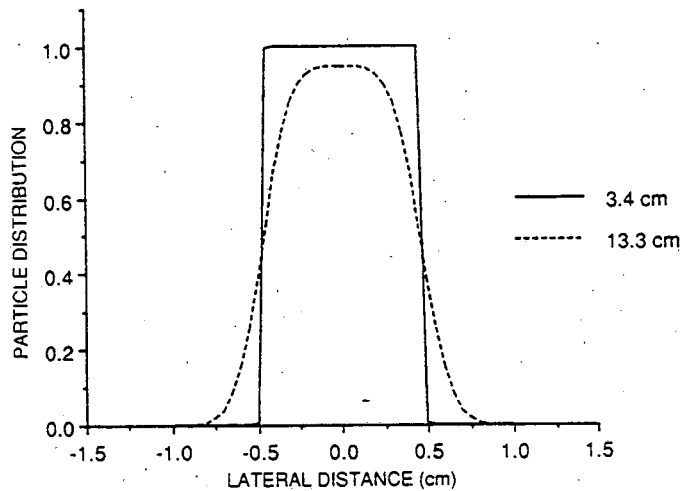
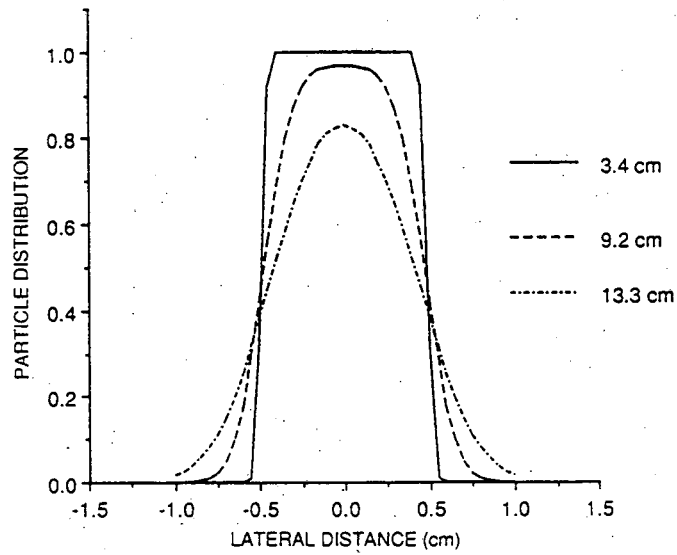


Figure 2.2: Particle distribution in a water bath of a beam of protons (*top*) and a beam of helium ions (*bottom*) perpendicular to the axis of the beam. Both beams have a range of 15 cm in water and are collimated by a 1 cm diameter aperture. The profiles are shown at depths of 3.4 cm, 9.2 cm, and 13.3 cm for the proton beam, and at 3.4 cm and 13.3 cm for the helium ions. For a given distance of penetration, the helium ions undergo less scattering and the beam exhibits sharper lateral edges relative to the proton beam.

CHARGED PARTICLES

accelerator was closed in 1988, and the LBL radiosurgical program continues, on a time-sharing basis with physics, at the Bevalac, a synchrotron capable of accelerating all ions from protons to uranium at energies from 100 to 2000 MeV/amu. Similarly, the Harvard cyclotron, a 160 MeV proton machine, was originally primarily a physics machine with some medical research, but is now completely dedicated to medical work. The proton accelerators in the Soviet Union all serve the dual purposes of physics research and medical treatments. They include: (1) the Moscow synchrotron (ITEP): 5 fixed energies between 70–200 MeV, (2) the Leningrad synchrocyclotron (LNPI): 1000 MeV, and (3) the Dubna synchrocyclotron (LNP of JINR). A dedicated medical proton accelerator has recently been built at Loma Linda, California and charged particle facilities for medical uses are being planned or already exist in Belgium, Canada, France, Germany, Japan, South Africa, Sweden, Switzerland, and at other locations in the U.S.

The exact nature of the accelerator, be it a cyclotron, synchrotron, or synchrocyclotron, determines the type of particles, their energy, and the time structure of the beam (e.g., whether the particles come in short, widely separated pulses, or more or less continuously). The type of accelerator also determines the dose rate of the machine, whether the energy is variable, and whether the beam can be shared between different users. All accelerators currently in use produce a beam that travels along a fixed horizontal axis. Beamport orientation is changed by rotating the patient about the fixed beam. The Loma Linda accelerator and future proton accelerators will couple the beam to a rotating gantry; magnets will bend the beam so that it can be delivered in an arc of 270° to 360°.

2.3.2 Tailoring the Beam

The charged particle beam must be tailored in several ways in order to make it usable for medical uses. These modifications fall under the following categories: (a) adjusting the range; (b) shaping the high-dose, Bragg peak region; and (c) shaping the beam laterally. Fig. 2.3 illustrates the treatment setup at LBL, including the beam-tailoring devices.

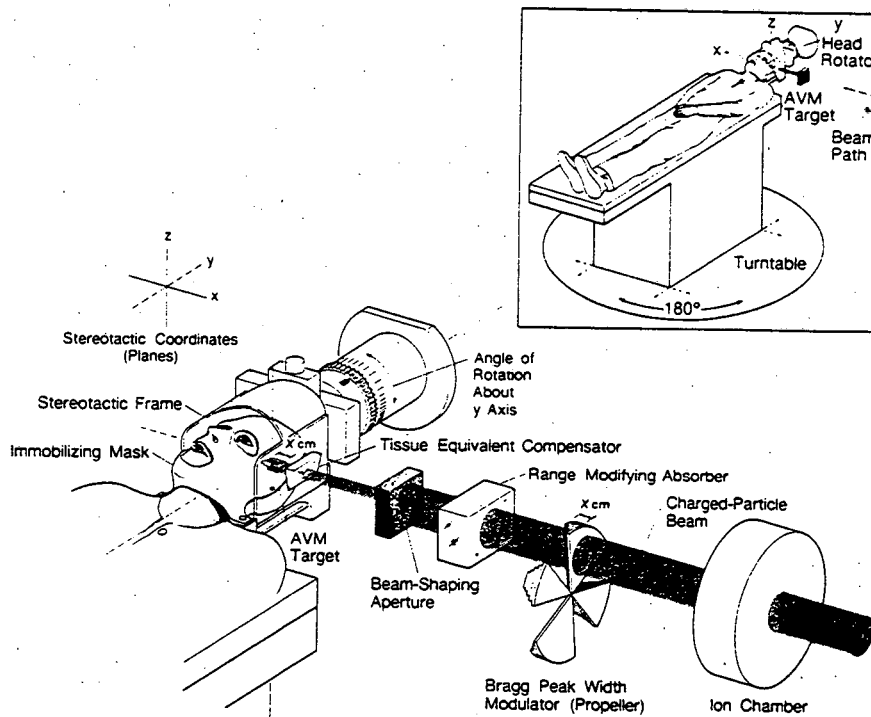


Figure 2.3: The patient is immobilized within the stereotactic mask and frame, which is attached to the patient positioner, ISAH (see Inset). The propeller modulates the width of the spread Bragg peak; the absorber modifies the particle range so that the Bragg peak will be placed at the target; the aperture shapes the beam to match the target volume projection; and the compensator tailors the distal edge of the Bragg peak to the distal edge of the target volume.

CHARGED PARTICLES

Range Adjustment

It is not practical to adjust the energy of the beam as it is extracted from the accelerator for every specific beamport range; the charged particle optics and the accelerator control system are too complicated. Normally, the extracted beam has one or a small number of fixed energies. If the Bragg peak is to be used for the treatment, then the energy of the beam must be degraded for each beamport so that the charged particles have the appropriate energy to pass through the head and stop precisely at the distal edge of the target volume. A variable thickness absorber such as sheets of polyethylene or a water-filled piston are commonly used.

If the plateau is to be used, one need only ensure that the beam energy is high enough that the Bragg peak lies outside the head. When the extracted beam energy is very high, the energy degradation may take place in two steps. The first is a fixed absorber that reduces the range to a fixed maximum for a given type of treatment. For example, at the 184" Synchrocyclotron at LBL, the 230 MeV/amu helium ion beam (31.6 cm range in water) was slowed down in 15 cm of polyethylene and 0.34 cm copper which resulted in a 145 MeV/amu beam with 14.5 cm range, sufficient for radiosurgical uses [29]. The thickness of a subsequent absorber was calculated and inserted for each individual beamport. The insertion of such energy absorbers increases the range straggling, so that the final Bragg peak is not as sharp, and can increase the penumbra of the beam. Care must be taken that collimators and beam-shaping apertures are placed to avoid scattered radiation from reaching the patient and to minimize a dose penumbra at the edges of collimators. If the absorbers are placed far upstream of the patient, then the penumbra is reduced. However, the particle flux at the patient, and hence the dose rate, is also reduced. The balance point in this trade-off depends on the particular accelerator set-up and treatment goals [27]. The energy absorbers commonly used are tissue-like substances, such as water, polyethylene, and lucite.

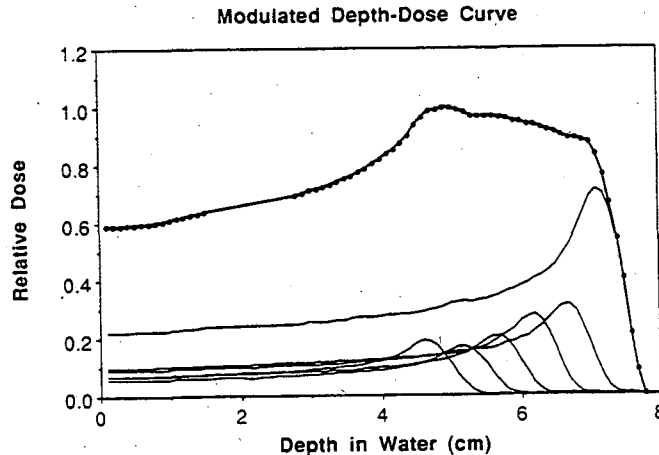


Figure 2.4: A 2.5 cm spread-out Bragg peak of helium ions with a range of 7 cm in water is plotted. The points are the measured values. The separate Bragg peaks that compose the spread peak are shown, with the height of each representing their relative weights. The physical dose is modified to account for the varying RBE of the helium ions, so that the relative biological effect is constant across the entire spread peak. The most distal peak has the highest weight of any of the beams in the spread peak.

Spread Bragg Peak

As Fig. 2.1 shows, the pristine Bragg peak is very narrow, on the order of millimeters. However, lesions to be treated—AVMs or tumors—can have dimensions on the order of centimeters. The Bragg peak region can be spread to conform to the size of the lesion by adding together a number of beams of slightly different range [2, 27, 29]. Fig. 2.4 shows how this can be accomplished. At LBL, two methods have been used. The first is by means of a propeller constructed of a number of sheets of lucite, each with wedges cut out. The fraction of the total circle that each wedge subtends is equal to the weight needed to achieve a uniform dose distribution when added to the dose delivered by the beams with shorter and longer ranges. When the propeller is spun very quickly in the beam, the required stacking of the beams is achieved. The second method is to use a variable wa-

CHARGED PARTICLES

ter column—a piston of water closed by two thin plexiglas windows. This can also be set to adjust the beamport range. The water thickness is set and a dose equal to the desired fraction for that beam is delivered. The beam is turned off, the water column set to the next range, and the procedure repeated until the desired dose has been delivered.

The dose due to charged particles is somewhat different than that due to x- or γ -rays owing to the different physical processes. This is a complex subject and for detailed information, the reader is referred to Reference [1]. Perhaps the biggest difficulty lies in determining the RBE of the Bragg peak of the charged particles. The RBE changes as a function of LET, and hence depth in the tissue. This variation is reflected in the non-uniform physical dose across the spread Bragg peak, as seen in Fig. 2.4. There is considerable debate over the RBE to use for protons, and the numbers range from 1 to 1.2. In order to account for the changing RBE with LET, values from the literature have been combined, and these are factored in when calculating the beam weights in the spread Bragg peak. At LBL, an overall RBE of 1.3 is used for helium ions in the central nervous system.

Lateral Beam Shaping

The shape of the beam in cross-section is determined by scatterers and apertures in the beamline. Normally, the beam delivered from the accelerator is Gaussian in shape and several centimeters in diameter. In order to produce a flat dose distribution over the desired 4 to 8 cm width, the beam passes through a lead or brass scatterer that increases the width of the Gaussian profile. However, this scattering results, as well, in undesired radiation beyond the edges of the treatment field; thick metal collimators along the beam line are used to shield the patient and equipment downstream. The beam is finally shaped to conform to the shape of the lesion by using a beam-shaping aperture at the surface of the patient. Fig. 2.5 illustrates the collimation of the beam by an individually shaped aperture. Designed for each beamport and constructed from a low-melting point, dense metal, these apertures block all particles outside the target volume.

Angular divergence of the beam as a result of the upstream scattering causes a penumbra around the edges of the aperture. Thus it is important that the aperture be placed as close to the patient as possible, and that the effective source of the particles—the upstream scatterer—be as far away from the patient as possible.

2.3.3 Dosimetry

A number of different charged particle detectors are used to determine the position of the beam, the dose delivered, and the uniformity of the beam. The dosimetric system at LBL [27] is described here; other accelerator dosimetry systems may vary in the particulars, but the principles remain the same [16]. Multi-wire proportional chambers located in the beamline measure the shape and position of the beam before it enters the treatment room. These are used to “tune” the beam into the area, ensuring reproducible beam location and shape. Two large, plane ionization chambers are used to determine the beam position, shape, and dose in the treatment room. The charge-collecting surfaces of these chambers can be divided into rings, quadrants, or strips in order to give position and beam-shape information. These are used to steer the beam during tuning and to monitor it during treatment. They are also used to monitor the dose on a continuous basis, the output going into charge-to-frequency converters. The output from these circuits controls the beam-clamping device to stop the beam when the desired dose is reached, either for the total treatment or for the particular beam in building a spread peak. A secondary electron emission monitor which does not saturate at high doses is also used as a safety precaution to monitor the dose.

Calibration of the physical dose delivered is achieved by using an NBS-calibrated, tissue-equivalent, thimble ionization chamber. For each beamport, the calibration chamber is placed behind an amount of polyethylene equivalent to the amount of tissue through which the charged particles must pass to reach the target volume. It is physically placed at the isocenter of the patient positioner and beam. These procedures ensure that the effects of beam divergence and scattering are accounted for. A predetermined number of counts

CHARGED PARTICLES

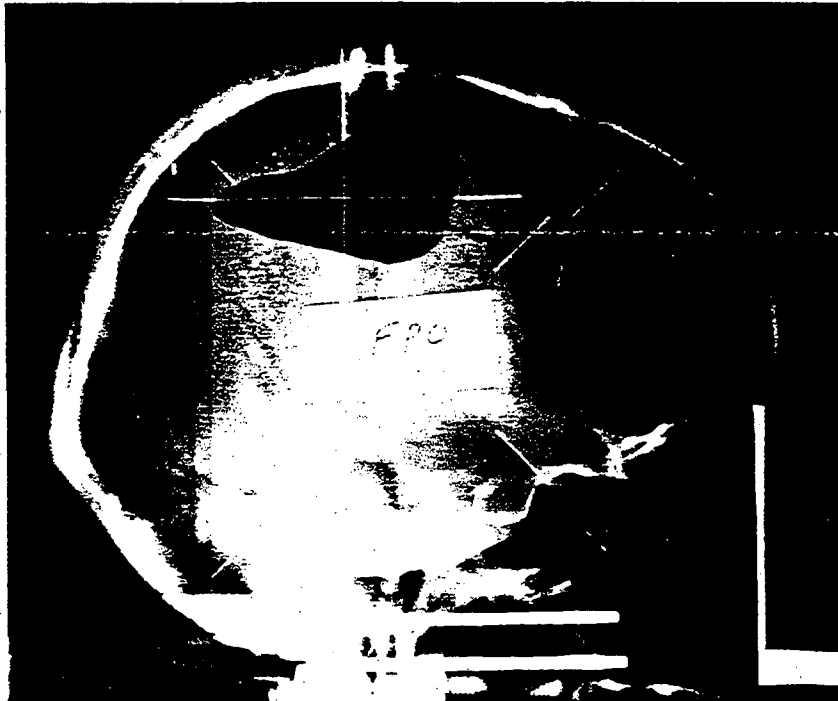


Figure 2.5: Positioning radiograph at the treatment facility. The stereotactic fiducial markers are visible as an "X". The center of the ion beam is demarcated by cross-hairs located in the area darkened by exposure of the film to a low-intensity helium ion beam that has been shaped with an individually-designed aperture.

is delivered to the upstream, plane ionization chambers. This is then compared with the measured dose on the calibration chamber and a calibration factor is calculated. This factor is used to calculate the number of counts on the upstream ionization chambers needed to deliver the desired dose to the target volume.

The beam uniformity, location, and shape after it has passed through the last aperture are measured using radiographic film. A cross-hair mounted on the beamline and coincident with the beam axis is used to check the location of the beam relative to the patient positioner. The film also serves to measure the beam penumbra at the edges of the aperture. (See Fig. 2.5.)

2.4 Target Localization

2.4.1 Stereotactic Imaging

The stereotactic method is presented in detail in Chapter 1. Stereotactic localization is not unique to any of the various radiosurgical methods using different radiations, and therefore will not be discussed here. Rather, this section deals with those aspects of target localization and patient positioning that are unique to charged particle radiosurgery.

The stereotactic frame used at LBL, pictured in Fig. 1.2, was designed to be easily removable rather than fixed to the bones of the skull [30]. This has several advantages. Since the accelerator is not hospital-based, a removable frame system makes it easy to perform the neuroradiological examinations elsewhere, and to eliminate the need for surgical facilities at the accelerator. This approach also provides time for the extensive treatment planning, beamline preparation, and target definition of large and complex lesions that is sometimes needed without causing excessive inconvenience or discomfort to the patient. That these factors are not limiting to the procedure, however, is witnessed by the fact that stereotactic radiosurgery is carried out at HCL-MGH using a more standard frame.

At LBL, stereotactic angiography and CT scanning are performed both for localization of the target volume and for use in treatment planning [38]. The LBL treatment planning (as will be

CHARGED PARTICLES

described below in Section 2.5) uses the CT image information to calculate charged particle energy loss in every pixel in the beamport. Since the target volume for AVMs is best imaged by angiography, the angiographic target information must be transferred to the CT images. This is accomplished by digitizing the stereotactic fiducial markers, the target volume, and bony landmarks as they appear on lateral and AP angiographic films. The fiducial marker positions are also recorded on the CT images. A computer program calculates the angiographic imaging magnification, rotation and position of the central ray from the digitized markers. Using the stereotactic information from the two angiographic projections, the program locates the digitized target contours in the stereotactic reference frame, calculates the transformation between the angiographic markers and the CT markers, and applies this transformation to the target contours. The projected widths and lengths of the AVM are used to define elliptical target contours on each of the corresponding CT slices. In this way a 3-dimensional target is built up in the CT images for calculation of the treatment plan. Tumors and selected vascular malformations are often better imaged on MRI than CT [6, 37]. An MRI-compatible frame allows the use of MRI imaging information in much the same way and the transformation of target contours from MRI images to the corresponding CT images.

At HCL-MGH, Bragg peak proton radiosurgery is carried out without such detailed, 3-dimensional calculations [13]. The relative homogeneity of the brain (with respect to charged particle energy loss) and the skull makes for a simple two-component system. Charged particle dose and range curves have been established to translate the position and size of the target (obtained from stereotactic images) into the required residual range and resulting dose for the proton beam. While this is less accurate than the method used at LBL, the successful clinical experience there provides a strong argument for its suitability. Confidence in this method also allowed the HCL-MGH program to perform Bragg peak radiosurgery before CT scanning was available.

The use of charged particle beams for the treatment of pituitary adenomas and conditions responsive to pituitary suppression at LBL, HCL-MGH, and the Soviet Union constitutes a large frac-

tion of the applications of charged particle radiosurgery [23]. The location of the pituitary is easily located by radiography because of its location in the bony sella. Using ventriculography to image the position of the optic nerve (often the limiting factor in irradiating the pituitary), these pituitary treatments were easily performed without the elaborate imaging that we currently have. Today, MRI is often used to evaluate the exact extent of the tumor so that a better dose distribution can be planned, thereby eliminating one of the major causes of treatment failure in the early days of charged particle radiosurgery.

2.4.2 Patient Positioning

The fixed horizontal beams of current medical accelerators require that the patient positioner have sufficient degrees of freedom to permit beamports from any desired orientation. The positioner should have three degrees of translational motion, and at least two degrees of rotational motion. (A third degree of rotation is achieved by rotating the shaped collimator about the beam axis.) The two axes of rotation intersect in a point which is also intersected by the axis of the charged particle beam. This point is called the *isocenter*. Any rotations of the patient about that point will still leave the beam directed at that center. The patient positioner at LBL (ISAH) is a very precise and versatile system that can accommodate a patient couch or chair; it is accurate to 0.1 mm in the three translational directions, and to 0.1° in rotation [28]. (See Fig. 2.3).

Positioning of the patient for treatment is accomplished by attaching the stereotactic frame to the treatment couch or chair, and adjusting the translational coordinates of the patient positioner so that the target volume center coincides with the isocenter. The patient positioner is then rotated in either one or both of the two rotational motions so that the beam trajectory coincides with the desired angle of entry. Once the stereotactic frame coordinates have been calibrated with respect to the patient positioner coordinates, patient positioning is very easy. The offset of the target volume center from the origin of the stereotactic frame coordinate system is calculated from the angiograms or CT images, and the corresponding

CHARGED PARTICLES

patient positioner coordinates calculated. Localization radiographs in the treatment position can be used to confirm the proper patient position.

The reliable use of the removable mask and stereotactic frame system at LBL requires somewhat more effort to confirm correct positioning than with a frame that is continuously attached to the patient's skull. The positioning of the patient proceeds as described above, but the initial patient position may be in error by several millimeters. Radiographs are taken of the patient in this position with X-ray tubes that have been precisely aligned to the axes and isocenter of the treatment system. These are compared with computer-generated overlays of the angiographic films (Fig. 2.6) [38]. The overlays are calculated from digitizations of the stereotactic fiducial markers, the target volume contours, and the midplane bony landmarks of the skull as they appear on the angiograms. The computer, using geometric optics, calculates the imaging parameters, and generates a real-sized overlay of these digitized points that corresponds to the magnification and other imaging parameters of the treatment-room radiographs. The localization radiographs are compared with the overlays, and the patient position is adjusted until the two correspond exactly. The error in this procedure is on the order of 1 mm [38]. Final positioning is achieved by exposing the x-ray film to a low-level beamspot so that the position and orientation of the beam-shaping aperture can be confirmed.

Potential errors can occur in several different manners. Repositioning the patient incorrectly is the most obvious, but as discussed above, relatively easy to correct. When using the Bragg peak, miscalculation of the charged particle range is an important potential source of error. This can occur for two reasons: (a) errors in the CT contours, and (b) errors in calculating charged particle energy loss. If the CT contour is misplaced in a direction perpendicular to the desired beamport, then the error in the calculated range for that beamport will usually be insignificant. If the contour is misplaced parallel to the beamport direction, then the range error is more or less equal to the error in contour placement. Such misplacement can also result in errors in compensator design, but such errors are usually small with respect to the compensator design resolution.

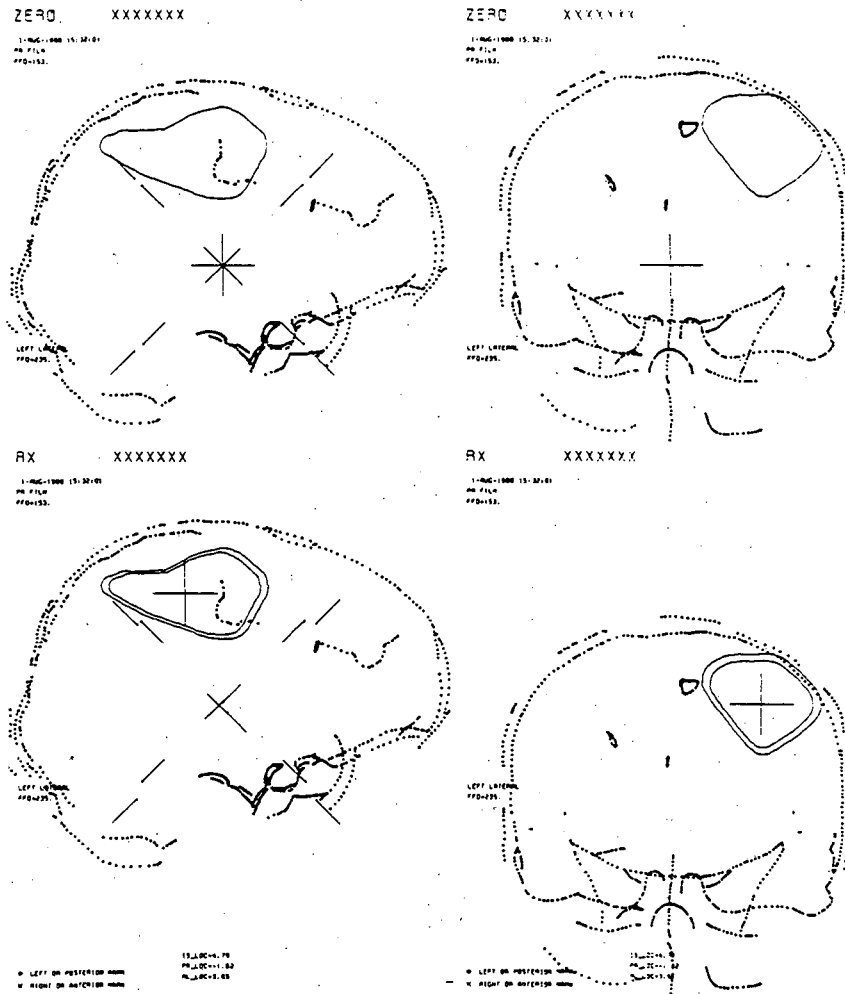


Figure 2.6: Computer-generated overlays of the angiographic films. Final positioning of the patient is achieved by overlaying these images with radiographs taken at the treatment site. The upper two images display the size and relative position of the structures and target projection when the patient is positioned with the frame center located at the isocenter. The bottom two images display the same information but with the patient positioned so the center of the target volume is located at isocenter.

CHARGED PARTICLES

At LBL, checks have been performed on repositioning errors using correlations between angiography, CT and MRI and looking at the relative positions of clearly identifiable structures such as the sella turcica. The error in the range due to these effects is no more than 1 mm. Range error resulting from miscalculation of charged particle energy loss will be discussed in the following section (2.5.1).

2.5 Treatment Planning

This section is devoted to describing the details of calculating isodose contours, as well as to discussing the dose distributions achieved in practice and the factors that affect them. Emphasis is given to the fundamental principles rather than details concerning one particular treatment planning procedure.

2.5.1 Calculation of Dose

Treatment Dose

Based on early work at LBL with respect to determining charged particle tolerance doses in the brain and on the experience of the Gamma Knife in the treatment of AVMs, maximal central target doses of 45 GyE were used in the beginning of the AVM program at LBL [5]. (GyE = Gray Equivalent = physical dose in Gy times the RBE of 1.3 in the Bragg peak. A dose of 45 GyE helium ions is a physical dose of 34.6 Gy.) This dose has been gradually lowered in steps as the efficacy of each dose level has been evaluated for AVM obliteration and incidence of complications. Doses between 45 GyE and 15 GyE (occasionally 10 GyE has been used in exceptional circumstances) have been explored, and current practice is to use doses of 25 GyE for small lesions and for lesions in less eloquent regions of the brain, and to use 15 to 20 GyE for large lesions and for those critically located. The doses quoted above refer to the dose delivered to the center of the target volume. The beamports are chosen and shaped so that the entire target volume receives at least 80% of the central dose.

For comparison, it should be noted that the Gamma Knife

K. Frankel

doses are usually given as the central dose with the dose at the edge of the lesion being 50% of the central dose. The figures presented here are the desired dose specifications. However, in practice with any radiosurgical system, errors in target localization and positioning, differences between the target volume and the high-dose region, and the steep dose fall-off of the dose distributions can result in delivered doses that differ from the ideal, specified doses.

The radiosurgery program at Harvard uses an empirically derived curve relating complications, dose, and target volume [12, 13]. A curve describing 1% complications is used to choose the dose, so that larger doses are used for small lesions and smaller doses for larger lesions. At the very largest lesion size, doses in the neighborhood of 10 Gy are used [12]. Although AVM obliteration may not occur frequently at such a low treatment dose, it is claimed that this dose provides some protection against hemorrhage [9].

Range Calculations

Previous sections have detailed the dose distribution characteristics of single beams of charged particles in a homogeneous water medium. The medical physicist is concerned with using these single beam characteristics for the calculation of the dose throughout the head resulting from a number of arbitrarily arranged beams. The first step is to calculate the dose from a beam of charged particles in an inhomogeneous medium that consists of the brain, with different components, and the skull. Compared with photons, this calculation is more critical with charged particles because of the Bragg peak and definite range of the particles. The contours of the target volume are not necessarily regular, and different parts of the charged particle beam traverse differing amounts of tissue, both brain and bone. Therefore, in order to achieve a uniform dose distribution within the target volume with steep dose gradients at its edges, care must be taken to calculate accurately the ranges of the charged particles as they traverse the head.

As discussed above in Section 2.2.1, charged particle energy loss is proportional to the electron density in the traversed medium. On the other hand, x-ray imaging, and in particular, CT, measure

CHARGED PARTICLES

the linear attenuation coefficient of a spectrum of x-rays in matter. At diagnostic energies, x-rays interact via the Compton effect and the photoelectric effect, the latter of which is very strongly dependent on the Z of the material ($\propto Z^3$). In order to relate the charged particle range to the CT numbers, the tissue is modelled as mixtures of two appropriate materials [2]. For CT numbers less than 0, the tissue is assumed to be a mixture of water and air; for numbers greater than 0, the mixture is of water and compact bone. Fat and very dense bones are two tissue components that pose problems for this model, but experiments with phantoms, animals, and humans have verified that a calibration of the charged particle range based on such a model is accurate to 3%.

In the treatment planning method developed at LBL for charged particles, the CT numbers (Hounsfield numbers) are converted to water-equivalent pathlength using an experimentally derived calibration curve and the two-component model described. Given a target contour, a beamport direction and the charged particle range in water before entering the patient, the computer program calculates the reduction in range pixel-by-pixel. Using a lookup table that tabulates the dose and lateral dose fall-off as a function of residual range in water, the dose distribution as a result of the beam is calculated for each pixel. This calculation, therefore, determines the amount of absorber one needs to insert into the beamline in order to adjust accurately the beamport range. This can be in the form of an absorber of uniform thickness across the beam profile, or a compensator shaped to match the entire distal surface of the beam to the contour of the target. The proton radiosurgical program at HCL-MGH determines the range by measuring the distance from the edge of the skull to the distal edge of the target on radiographic films and converting the distance to charged particle range using experimentally derived calibration curves that account for the different energy losses in brain and bone [13]. The effects of multiple scatteringscattering!multiple Coulomb on the dose for different collimator sizes are calculated in a similar fashion.

Irradiation Geometry

The number, orientation, and weighting of beamports depends on the size, shape, and location of the lesion as well as on the particular radiosurgical technique practiced at an institution. Plateau irradiation with charged particle beams requires an irradiation geometry that uses a large number of ports or several intersecting arcs. In this sense, plateau irradiation is quite similar to stereotactic irradiation with the Gamma Knife or linear accelerator arc method. The Bragg peak method requires many fewer ports to achieve similar dose localization—usually between 4 and 12 ports. In the Soviet Union, plateau irradiation is used for target volumes smaller than 1.5 cm in diameter in order to make use of the sharp lateral fall-off in dose in the plateau region; for larger target volumes, the Bragg peak method is used [34]. The programs at LBL and HCL-MGH use the Bragg peak for all lesions, although the pituitary radiosurgery program at LBL used the plateau beam from 1954 to 1980.

The number of beams used in Bragg peak procedures depends also on the extent to which each beamport is modified by beam-shaping apertures, spreading of the Bragg peak, and compensators. Using all of these techniques, the procedure at LBL is to use approximately 4 beamports per target volume. Small lesions (less than 2 cm diameter) can usually be treated readily by 4 beams, typically confined to the affected hemisphere of the brain. These beams lie between 20° and 30° from the orthogonal lateral axis in the anterior, posterior, superior, and inferior directions. Fig. 2.7 shows a small (1.0 cm³) right parietal AVM that was treated with four 1.6 cm diameter beams with a 1.08 cm spread Bragg peak. The entire target is enclosed within the 90% isodose surface for this case. In general, beam-shaping is used to enclose the target within the 80% or higher isodose surface. This figure illustrates the extent to which charged particles can completely spare most of the normal brain tissue from any radiation.

The treatment plan is illustrated with two orthogonal sections: (top) axial and (bottom) coronal. The isodose contours, which represent the 100, 90, 50, 10, and 1% dose contours, account only for those beams that lie within the respective plane. Therefore, in the

CHARGED PARTICLES

axial view, only the right temporal anterior and the right temporal posterior beamports contribute to the isodose contours shown. Similarly, in the coronal view, only the right temporal superior and right temporal inferior beams are calculated. In the region of the target volume where all of the beams intersect, the isodose contours shown in the figure are good approximations to those that would be calculated with all (non-coplanar) beams. In those areas where there is no overlap, the displayed contours are too large by approximately a factor of 2.

Fig. 2.8 illustrates a similarly sized lesion (0.80 cm^3) that is more centrally located in the thalamus, here treated with four $1.6 \text{ cm} \times 1.2 \text{ cm}$ shaped beams using a 1.08 cm spread peak. Lesions that lie in the midplane of the brain are typically treated with 2 beams from each side of the head (left anterior and posterior, right anterior and posterior). This is illustrated in Fig. 2.9 in the treatment of a deep posterior fossa AVM (0.33 cm^3) with four, discrete $1.0 \text{ cm} \times 0.8 \text{ cm}$, 1.08 cm -spread beams.

Treatment of larger lesions is planned on an individual basis using a combination of beams along or oblique to the lateral, posterior, and anterior axes. If the lesion lies wholly within one hemisphere, the beams are confined to that hemisphere if possible. Even large, irregularly-shaped lesions can be treated in this fashion as long as the aforementioned beam-shaping techniques are used. At Harvard, these techniques are not used to the same degree, and often up to 12 beams are used, arranged bilaterally about the lateral axis [13].

Fig. 2.10 is a representative example of a medium-sized lesion. Four beams are arrayed about the lateral direction for the treatment of a 4.0 cm^3 deep left thalamic AVM. The beam-shaping aperture had maximum dimensions of $2.4 \text{ cm} \times 1.9 \text{ cm}$ and the Bragg peak was spread 2.16 cm . The 90% isodose contour matches the target volume boundary and the unaffected hemisphere receives virtually no radiation.

Fig. 2.11 illustrates the use of beamports from the anterior and posterior directions. A 18.0 cm^3 AVM located in the left thalamus and internal capsule is treated with 2 ports from the left side ($4.4 \text{ cm} \times 2.8 \text{ cm}$, 2.0 cm spread peak), one from the superior posterior direction ($3.2 \text{ cm} \times 2.8 \text{ cm}$, 3.6 cm spread peak), and one from the

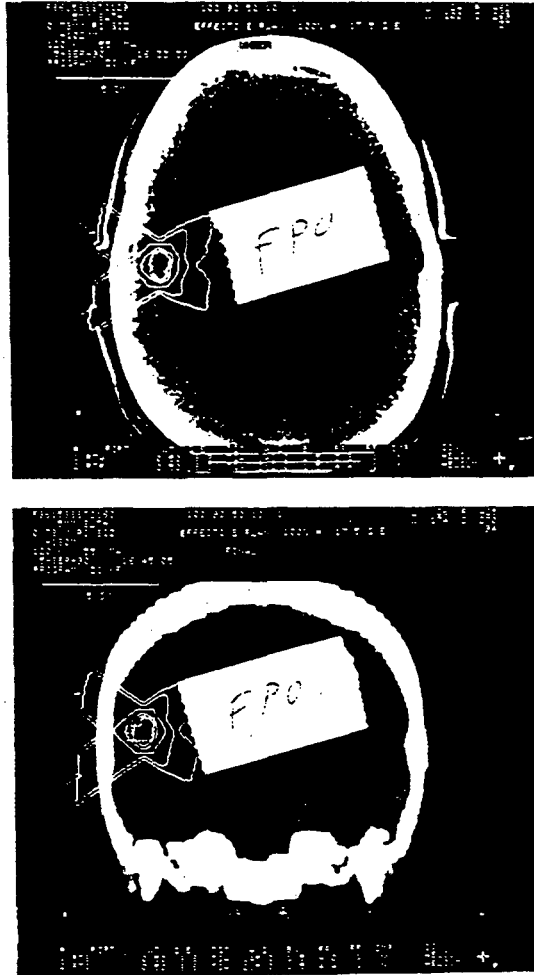


Figure 2.7: A small (1.0 cm^3) right parietal opercular AVM was treated with four oblique beams from the right side. The beamports were shaped using a 1.6 cm diameter circular aperture and the Bragg peak was spread 1.08 cm. The central dose was 35 GyE. The target contour on this CT slice is delineated by the dotted line. The isodose contours are shown for 100, 90, 50, 10, and 1% of the maximum central dose. *Top*: Axial CT view through the center of the lesion showing the right temporal anterior and right temporal posterior beamports. They are angled $\pm 32^\circ$ from the lateral axis. *Bottom*: Coronal reconstructed CT view through the center of the lesion showing the right temporal superior and right temporal inferior beamports at $\pm 35^\circ$.

CHARGED PARTICLES

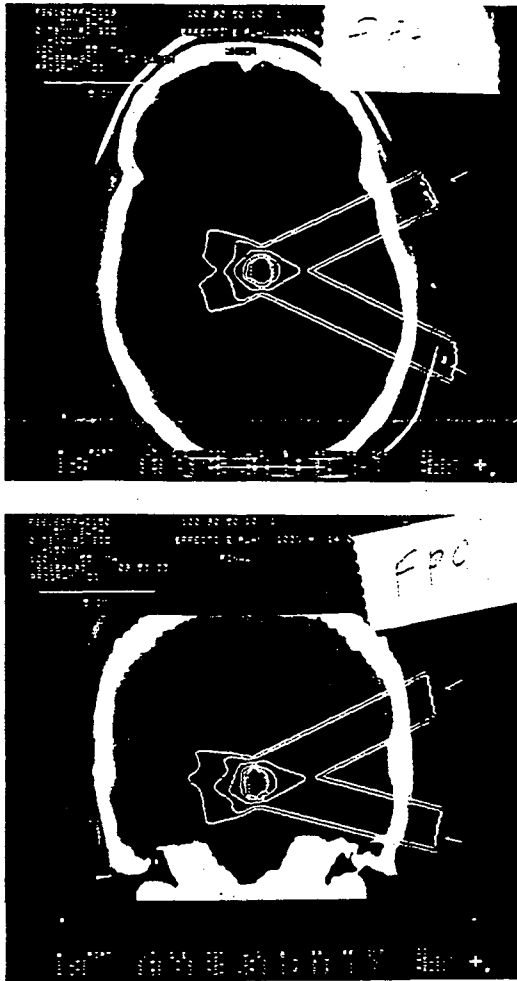


Figure 2.8: A 0.80 cm^3 lesion located in the thalamus is treated with four beams from the left side. Each beamport was collimated with a shaped beamport whose greatest dimensions were $1.6 \text{ cm} \times 1.2 \text{ cm}$; the Bragg peak was spread 1.08 cm . The central dose was 28 GyE . The isodose contours are shown for 100, 90, 50, 10, and 1% of the maximum central dose. *Top*: Axial CT view through the center of the lesion showing the left temporal anterior and left temporal posterior beamports. They are angled $\pm 25^\circ$ from the lateral axis. *Bottom*: Coronal reconstructed CT view through the center of the lesion showing the left temporal superior and left temporal inferior beamports at 25° and -15° , respectively.



Figure 2.9: A small (0.33 cm^3) lesion lying in the center of the posterior fossa is treated by two beams from the left side and two beams from the right side of the head. The beamports were collimated with a $1.0 \text{ cm} \times 0.85 \text{ cm}$ elliptical aperture and the Bragg peak was spread 1.08 cm . The central dose was 15 GyE . The isodose contours are shown for 100, 90, 50, 10, and 1% of the maximum central dose. *Top*: Axial CT view through the center of the lesion showing the left temporal posterior and right temporal posterior beamports. They are angled -33° and -30° from the lateral axis. *Bottom*: Coronal reconstructed CT view through the center of the lesion showing the left temporal superior and right temporal superior beamports at $\pm 30^\circ$.

CHARGED PARTICLES

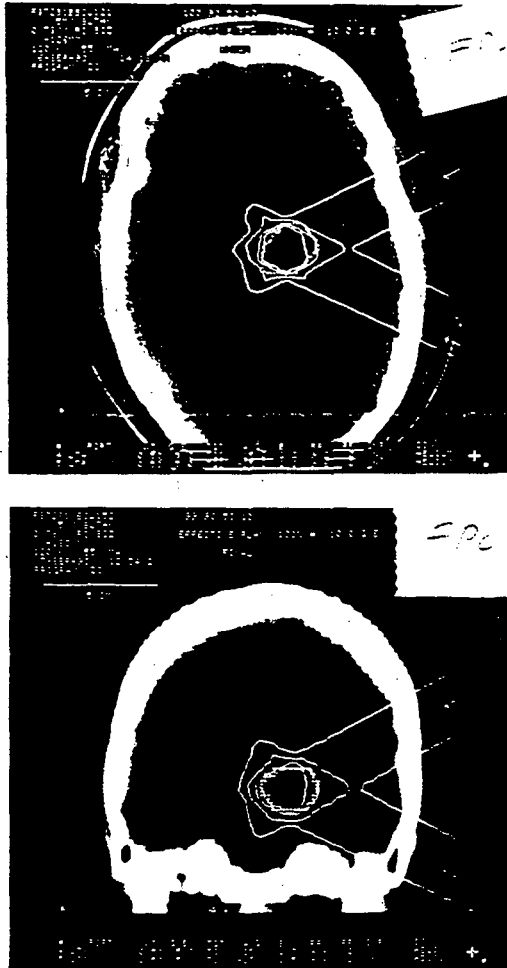


Figure 2.10: A medium-sized lesion (4.0 cm^3) is treated in a similar fashion to the smaller lesions shown in Fig. 2.7 and 2.8. The beams were shaped with an individually shaped collimator with dimensions of $2.4 \text{ cm} \times 1.9 \text{ cm}$ and a spread Bragg peak of 2.16 cm . The central dose was 16 GyE . The isodose contours are shown for 100, 90, 50, and 10% of the maximum central dose. *Top*: Axial CT view through the center of the lesion showing the left temporal anterior and left temporal posterior beamports. They are angled $\pm 25^\circ$ from the lateral axis. *Bottom*: Coronal reconstructed CT view through the center of the lesion showing the left temporal superior and left temporal inferior beamports at $\pm 27^\circ$.

superior anterior direction (3.2 cm x 2.8 cm, 3.6 cm spread peak)).

Fig. 2.12 is a similar case but with one beam coming from the right side. This 40.0 cm³ deep left frontal and parietal AVM is treated with a left and a right lateral (8.0 cm x 5.8 cm, 2.16 cm spread peak), an anterior, and a posterior (5.9 cm x 2.5 cm, 4.0 cm spread peak) beamport. The distal edge of the Bragg peak of each beamport is shaped with a compensator in order to match the isodose contours with the target boundary in the presence of varying amounts of dense bone and soft tissue. The treatment plans shown in Fig. 2.11 and 2.12 are good illustrations of the ability of charged particles to conform the high dose region to even very large target volumes while sparing normal tissue.

Fig. 2.13 illustrates a 3-dimensional treatment plan of a 17.0 cm³ left thalamic and basal ganglia AVM using 4 non-coplanar beams. The beams were collimated with 4.6 cm x 4.2 cm (left temporal beamport) and 4.2 cm x 3.3 cm (left posterior superior, left posterior inferior, and left anterior superior beamports) shaped apertures, and the Bragg peaks were spread 3.0, 3.5, 2.5 and 2.5 cm, respectively. The isodose contours illustrated in this figure were calculated taking into account all non-coplanar beams. The calculations were performed on a 0.32 cm x 0.32 cm x 0.30 cm grid on a set of CT scans spanning the entire head. Such a 3-D calculation provides a much more accurate set of isodose contours, especially with larger lesions, and is quite valuable in evaluating competing treatment plans.

Treatment Plan Evaluation

The evaluation of treatment plans is an important, but inexact procedure. The range of possible treatment plans is a function of the radiosurgical method used and may require compromises from what the physician would ideally wish to have. They also incorporate any imprecision or uncertainty in identifying the exact extent of the lesion that results from imaging limitations. Finally, they are a function of the type of treatment planning process used.

Two methods of charged particle treatment planning have been discussed—one based on measurements made on angiograms of bone and soft tissue dimensions, and one based on pixel-by-pixel evalua-

CHARGED PARTICLES

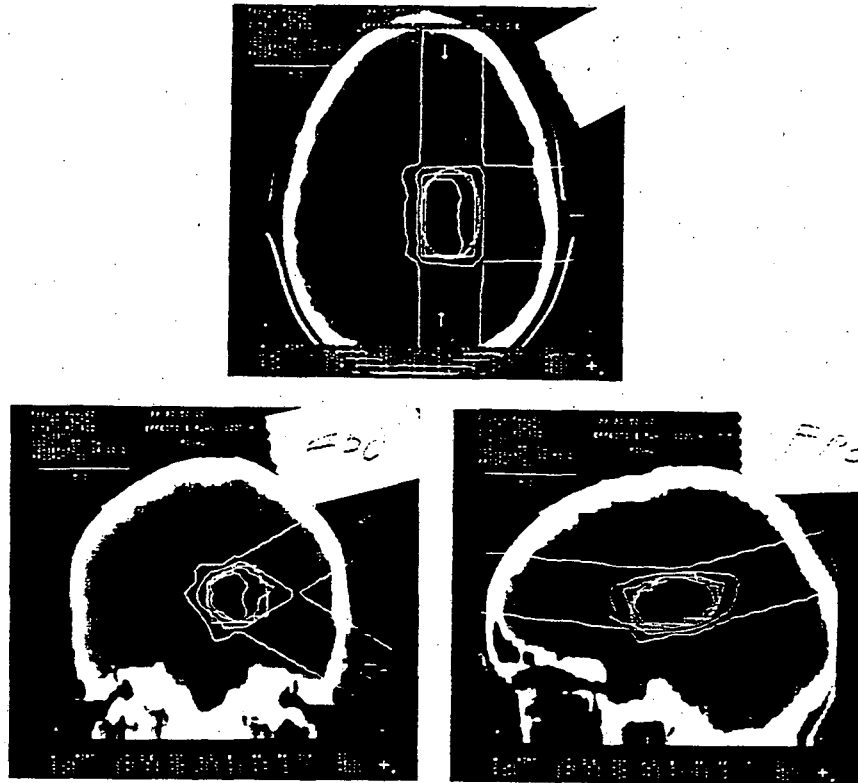


Figure 2.11: A large (18.0 cm^3) lesion requires the use of ports from the anterior and posterior directions in addition to two lateral ports. The lateral ports were collimated with a $4.4 \text{ cm} \times 2.8 \text{ cm}$ collimator with a 2.0 cm spread Bragg peak. The posterior and anterior ports were shaped with a $3.2 \text{ cm} \times 2.8 \text{ cm}$ collimator and with a 3.6 cm spread Bragg peak. The central dose was 15 GyE . The isodose contours are shown for 99, 90, 50, and 10% of the maximum central dose. *Top center:* The beamports shown do not represent actual ports but instead are projections of the ports onto the central axial plane. *Bottom left:* Reconstructed coronal CT view with the left temporal superior and left temporal inferior beamports ($\pm 30^\circ$). *Bottom right:* Reconstructed sagittal CT view with the left posterior superior (15°) and left anterior superior (5°) beamports.

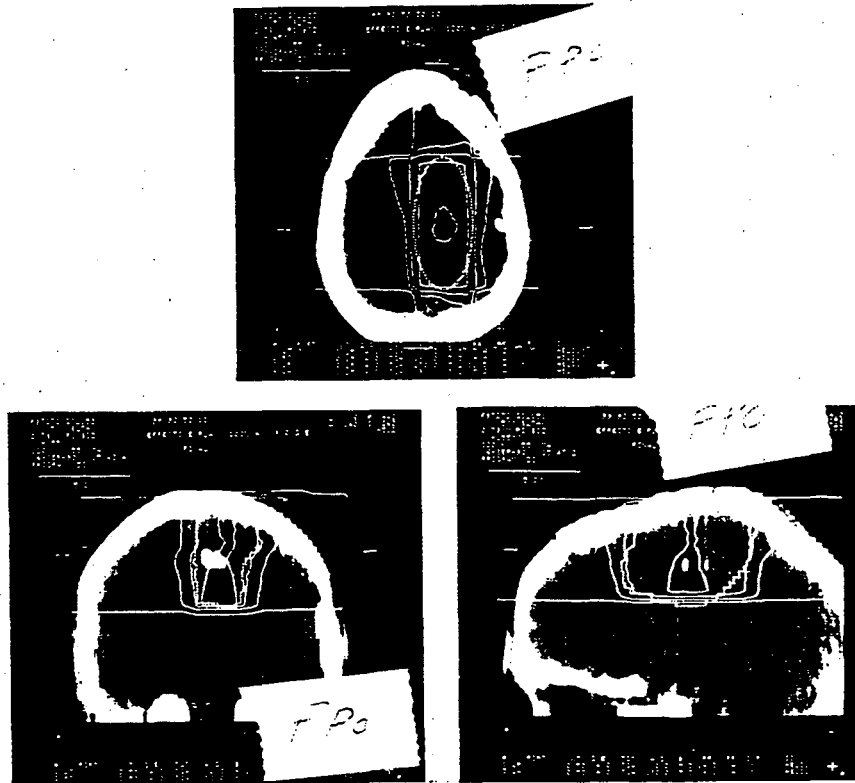


Figure 2.12: A very large lesion (40.0 cm^3) is shown treated with four beams from the right lateral, left lateral, posterior, and anterior axes. The lateral beams were shaped with a $8.0 \text{ cm} \times 5.8 \text{ cm}$ collimator and spread 2.16 cm . The posterior and anterior beams were shaped with a $5.9 \text{ cm} \times 2.5 \text{ cm}$ collimator and spread 4.0 cm . Isodose contours of 99, 90, 50, and 10% are shown. The sagittal and coronal views illustrate the use of compensators (made of lucite) to adjust the shape of the distal edge of the Bragg peak to account for target shape and varying amounts of bone and soft tissue.

CHARGED PARTICLES

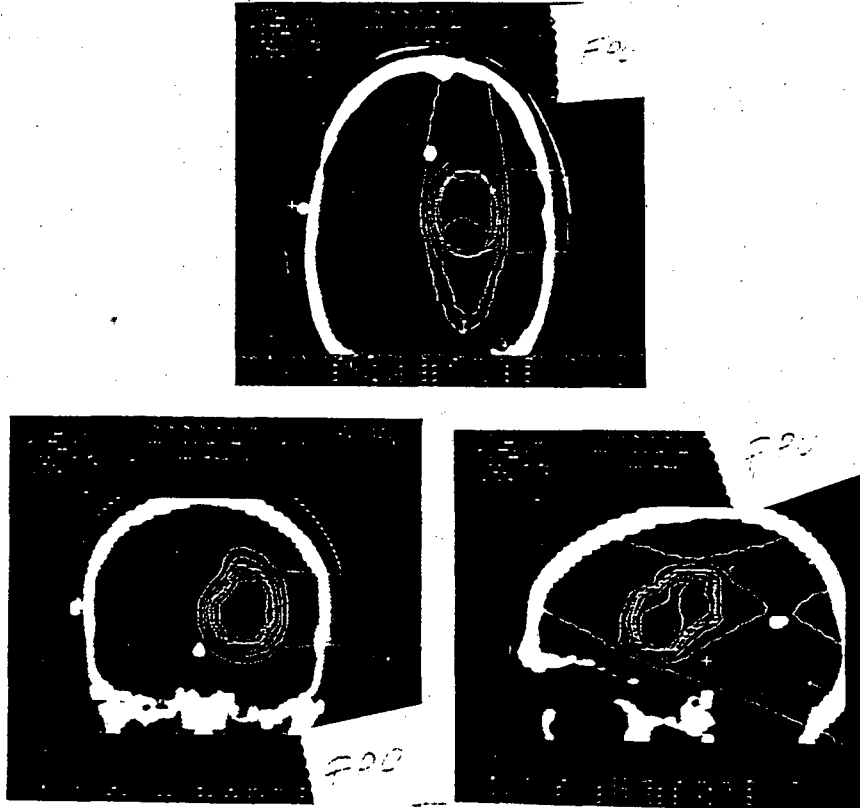


Figure 2.13: A 17.0 cm^3 AVM located in the left globus pallidus and internal capsule is treated with four beams. The ports used were left temporal, left posterior superior, left posterior inferior, and left anterior superior. These beams were shaped using $46 \text{ cm} \times 42 \text{ cm}$ (LT) and $.42 \text{ cm} \times 33 \text{ cm}$ (LPS, LPI, LAS) collimators, and the widths of the spread Bragg peaks were 3.0, 3.5, 2.5, and 2.5 cm. The isodose contours (99, 90, 70, 50, 30, and 10%) have been calculated with a 3-D program and reflect the dose contributions of non-coplanar ports. Beamshaping compensators were used but are not visible on these images.

tion of charged particle energy loss. Using the first method, treatment plans can be evaluated only in general terms, and cannot take into account individual differences. Important parameters such as the rate of dose fall-off in the distal and lateral directions for particular values of lesion depth and beamwidth can be obtained by application of calibrations made in phantoms. However, the exact relationship between the dose distribution and the target volume cannot be obtained.

Using CT-based calculations, the relationship between dose distribution and target volume can be quantified. They can be quantified in 1-, 2-, or 3-dimensions. In 1-D, the dose along a ray through the target volume can be calculated and displayed along with the dimension of the target. These dose profiles are often given along the three principle axes. A 2-D display of isodose contours overlaid on the CT image, along with the target contour, provides much more information, and is particularly useful for evaluating the match between the dose distribution and irregularly shaped targets. Such displays are of great importance in designing compensators and determining the desired spread of the Bragg peak in charged particle radiosurgery. If treatment plans have been calculated on all of the CT slices that contain the target volume, then a 3-D representation of the dose can be given by means of dose-volume histograms. These histograms show the number of voxels (3-D volume elements) that receive a particular dose. The volume considered can be the target volume, the entire brain, the entire brain minus the target volume, or any brain structure that has been defined by contouring. With these plots, treatment plans can be compared by examining the uniformity of the dose distribution to the target volume, and the dose to normal structures [36].

Fig. 2.14 is an integral dose-volume histogram for the target volume for the treatment of a 2 cm diameter spherical target located in the center of the brain. The value of the ordinate at any given point represents the fraction of the brain that has received at least as much dose as shown on the abscissa. The histogram shows that protons, carbon ions, and photons can all give uniform coverage to the target volume. Fig. 2.15 is an integral histogram of the entire brain (excluding the target volume) for the treatment of a 5 cm³ and

CHARGED PARTICLES

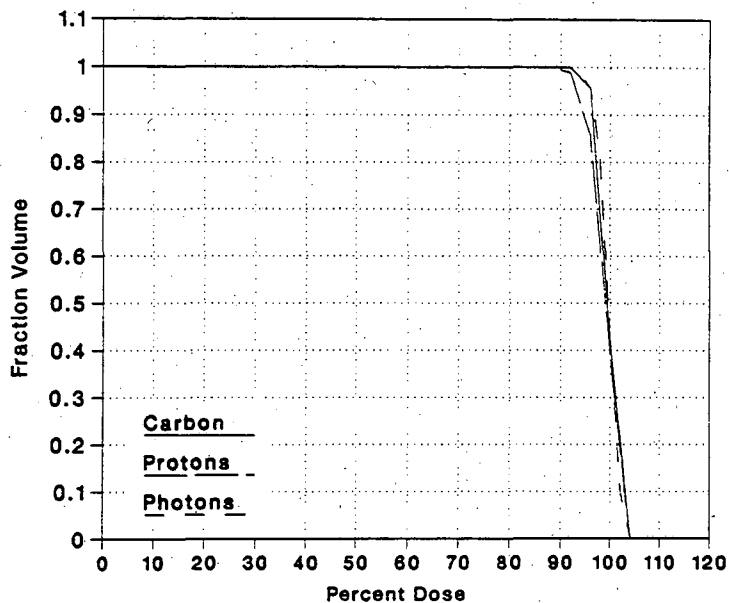


Figure 2.14: Integral dose-volume histograms calculated for a 2 cm diameter spherical target located in the center of the brain. Histograms are calculated for protons, carbon ions, and photons. The ordinate has been scaled to a total volume of 1; the actual volume is 4.2 cm³. The plot shows the fraction of the total target volume that receives at least a given percentage of the prescribed dose.

a 56 cm³ spherical volume. The photon treatment plan (calculated using the Heidelberg Linac geometry) results in more dose to the normal brain than the helium ion plan for both sizes of lesions, but the difference is substantially greater for the larger target volume.

Fig. 2.16 plots the dose-volume histogram for the dose received by the brain stem for a 28 cm³ located in the right caudate and putamen anteriorly and in the globus pallidus and thalamus posteriorly. Again, a significant difference is seen between the charged particle and the photon treatment plans.

Three-dimensional treatment planning programs enable the calculation of isodose contours and dose-volume histograms for treatment plans that contain non-coplanar beamports, and such a program was used to calculate all of the histograms shown in this chap-

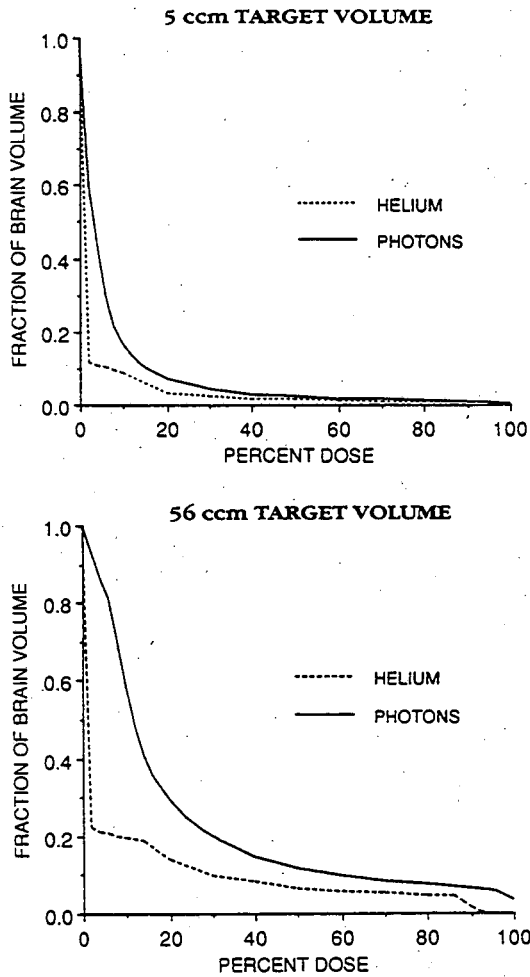


Figure 2.15: Integral dose-volume histograms calculated for the entire brain (volume, 1300 cm³) for the treatment of a 5 cm³ (top) and a 56 cm³ (bottom) centrally-located lesion. The histograms are shown for helium ions and photons. The differences between the dose delivered to the brain by helium ions and by photons is relatively minor for a small lesion. The difference is much greater for a large lesion.

CHARGED PARTICLES

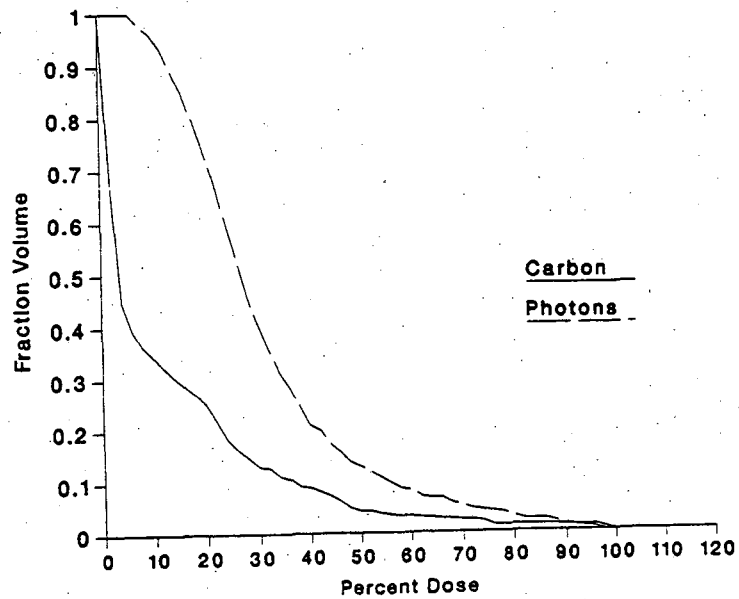


Figure 2.16: Integral dose-volume histograms calculated for the brainstem using carbon ions and photons. The target was a 28 cm³ lesion located in the right caudate and putamen anteriorly and the globus pallidus and thalamus posteriorly. The target volume and the contoured volume of the brainstem did not overlap. There is virtually no difference between helium ions and carbon ions for this histogram.

ter. Such considerations are more important for charged particle radiosurgery than for photon radiosurgery since aperture shapes, compensators and the effects of inhomogeneities on the location of the Bragg peak can result in hard-to-visualize dose distributions. Three-dimensional calculations are more important for evaluating treatment plans for larger lesions than for smaller ones. Clearly, if the target volume only contains a small number of voxel elements, the resolution of the calculations will limit the useful information, and differences between dose distributions and target contours will be somewhat uncertain. However, it must be recognized that a 3-dimensional, voxel by voxel treatment plan is more accurate than any other method regardless of target size or beamport orientations.

2.6 Strengths and Weaknesses

Charged particles applied to stereotactic radiosurgery have the following strengths relative to other modalities.

1. The Bragg peak, either spread or pristine, delivers more dose at depth relative to the surface dose than do photons. Many fewer beamports are needed to localize the high dose region within the target volume.
2. The sharp distal edge of the Bragg peak (resulting from the well-defined range-of penetration of a monoenergetic beam of particles) allows the use of range-modifying devices to tailor the distal edge of the high-dose region to the shape of the target volume.
3. The ability to stack Bragg peaks to form a uniform region of dose allows for the tailoring of the high-dose region to the length of the target volume.
4. The use of 3-6 beamports makes it feasible to use individually-shaped apertures for each beamport so that the profile of the charged particle beam conforms precisely to the target profile.

CHARGED PARTICLES

5. The above-mentioned physical characteristics result in the ability to treat large (greater than 2 cm in diameter) and irregularly-shaped lesions with a uniform dose while sparing much more normal tissue than is possible with photon methods.
6. The high-dose rate and low number of beamports results in a treatment time of 1-5 minutes per port with a total treatment time, including patient alignment, of 30 to 90 minutes.

The weaknesses of the charged particle stereotactic radiosurgery method are as follows.

1. The accelerators used to produce the high energy charged particle beams are more costly than photon sources and require more technically difficult design and maintenance.
2. The need to calculate charged particle energy loss on a pixel by pixel basis increases the treatment planning time and introduces some potential error in converting from CT values to charged particle stopping power.
3. The use of individual beam-modifying devices increases the preparation time for each patient's treatment relative to photon methods.
4. The relative biological effectiveness of charged particles in the different areas of the brain is not known precisely so that comparison with photon irradiation experience is hindered.

Acknowledgments

This work was supported, in part, by Grant 7 RO1 CA51076 from the National Cancer Institute and by the Office of Energy, Health, and Environmental Research of the U.S. Department of Energy, contract DE-AC03-76SF00098.

K. Frankel

References

- [1] FH Attix, WC Roesch, E Tochilin. *Radiation Dosimetry*. Academic Press, Inc., New York, 1968.
- [2] GTY Chen, RP Singh, JR Castro, JT Lyman, JM Quivey. Treatment planning for heavy ion radiotherapy. *Int J Radiat Oncol Biol Phys*, 5:1809-1819, 1979.
- [3] JI Fabrikant, KA Frankel, MH Phillips, RP Levy. Stereotactic heavy charged-particle Bragg peak radiosurgery for intracranial arteriovenous malformations. In MSB Edwards and HJ Hoffman, editors, *Cerebral Vascular Diseases of Childhood and Adolescence*, chapter 22, Part 2, pages 389-410. Williams and Wilkins, 1989.
- [4] JI Fabrikant, RP Levy, MH Phillips, KA Frankel, JT Lyman. Neurosurgical applications of ion beams. *Nuclear Instruments and Methods in Physics Research*, B40/41:1376-1384, 1989.
- [5] JI Fabrikant, JT Lyman, Y Hosobuchi. Stereotactic heavy-ion Bragg peak radiosurgery: Method for treatment of deep arteriovenous malformations. *Br J Radiol*, 57:479-490, 1984.
- [6] VB Graves and TA Duff. Intracranial arteriovenous malformations current imaging and treatment. *Investigative Radiology*, 25:952-960, 1990.
- [7] B R Griffin, S Hummel Warcola, M R Mayberg, J Eenmaa, J Eskridge, H R Winn. Stereotactic neutron radiosurgery for arteriovenous malformations of the brain. *Medical Dosimetry*, 13: 179-182, 1988.
- [8] RN Kjellberg, KR Davis, S Lyons, W Butler, RD Adams. Bragg peak proton beam therapy for arteriovenous malformations of the brain. *Clinical Neurosurgery*, 31:248, 1983.
- [9] RN Kjellberg, T Hanamura, KR Davis, SL Lyons, RD Adams. Bragg peak proton beam therapy for arteriovenous malformations of the brain. *N Engl J Med*, 309:269-274, 1983.
- [10] RN Kjellberg and B Kliman. Lifetime effectiveness—a system of therapy for pituitary adenomas, emphasizing Bragg peak proton hypophysectomy. In JA Linfoot, editor, *Recent Advances in the Diagnosis and Treatment of Pituitary Tumors*, pages 269-288. Raven Press, New York, 1979.

- [11] RN Kjellberg, JW McMeel, NL McManus. Pituitary suppression in diabetic retinopathy by proton beam in surgically unfit patients. In MF Goldberg and SL Fine, editors, *Symposium on the Treatment of Diabetic Retinopathy*, pages 249-276. Airlie House (U S Public Health Service Publ. No. 1890), Arlington, VA, 1968.
- [12] RN Kjellberg. Isoeffective dose parameters for brain necrosis in relation to proton radiosurgical dosimetry. In G Szikla, editor, *Stereotactic Cerebral Irradiation, INSERM Symposium No. 12*, pages 157-166. Elsevier/North-Holland Press, 1979.
- [13] RN Kjellberg. Stereotactic Bragg peak proton radiosurgery method. In G Szikla, editor, *Stereotactic Cerebral Irradiation, INSERM Symposium No. 12*, pages 93-100. Elsevier/North-Holland Press, 1979.
- [14] B Kliman, RN Kjellberg, B Swisher, W Butler. Proton beam therapy of acromegaly: a 20-year experience. *Prog Endocr Res Ther*, 1:191-211, 1984.
- [15] B Larsson, K Liden, B Sarby. Irradiation of small structures through the intact skull. *Acta Radiologica: Therapy, Physics, Biology*, 13:512-534, 1974.
- [16] B Larsson and B Sarby. Equipment for radiation surgery using narrow 185 MeV proton beams: Dosimetry and design. *Acta Oncologica*, 26:143-158, 1987.
- [17] JH Lawrence. Heavy particle irradiation of intracranial lesions. In RH Wilkens and SS Rengachary, editors, *Neurosurgery*, pages 1113-1132. McGraw-Hill, New York, 1985.
- [18] JH Lawrence and JA Linfoot. Treatment of acromegaly, Cushing disease and Nelson syndrome. *West J Med*, 133:197-202, 1980.
- [19] JH Lawrence, CA Tobias, JA Linfoot, JL Born, A Gottschalk, RP Kling. Heavy particles, the Bragg curve and suppression of pituitary function in diabetic retinopathy. *Diabetes*, 12:490-501, 1963.
- [20] JH Lawrence, C Tobias, JL Born, CC Wang, JH Linfoot. Heavy-particle irradiation in neoplastic and neurologic disease. *J Neurosurg*, 19:717-722, 1962.
- [21] L Leksell. The stereotaxic method and radiosurgery of the brain. *Acta Chir Scand*, 102:316-319, 1951.
- [22] L Leksell, B Larsson, B Andersson, B Rexed, P Sourander, W Mair. Lesions in the depth of the brain produced by a beam of high energy protons. *Acta Radiol*, 54:251-264, 1960.
- [23] RP Levy, JI Fabrikant, KA Frankel, MH Phillips. Particle beam radiosurgery. In W Friedman, editor, *Neurosurgery Clinics of North America*. W.B. Saunders, Philadelphia, pp. 955-990: 1990.
- [24] RP Levy, JI Fabrikant, KA Frankel, MH Phillips, JT Lyman. Stereotactic heavy-charged-particle Bragg peak radiosurgery for the treatment of intracranial arteriovenous malformations in childhood and adolescence. *Neurosurgery*, 24:841-852, 1989.

CHARGED PARTICLES

- [25] JA Linfoot. Heavy ion therapy: alpha particle therapy of pituitary tumors. In JA Linfoot, editor, *Recent Advances in the Diagnosis and Treatment of Pituitary Tumors*, pages 245-267. Raven Press, New York, 1979.
- [26] JA Linfoot, JH Lawrence, JL Born, CA Tobias. The alpha particle or proton beam in radiosurgery of the pituitary gland for Cushing's disease. *N Engl J Med*, 269:597-601, 1963.
- [27] B Ludewigt, W Chu, M Phillips, T Renner. Accelerated helium-ion beams for radiotherapy and stereotactic radiosurgery. *Medical Physics*, 13: 36-42, 1991.
- [28] JT Lyman and CY Chong. ISAH: a versatile treatment positioner for external radiation therapy. *Cancer*, 34:12-16, 1974.
- [29] JT Lyman, L Kanstein, F Yeater, JI Fabrikant, KA Frankel. A helium-ion beam for stereotactic radiosurgery of central nervous system disorders. *Medical Physics*, 13:695-699, 1986.
- [30] JT Lyman, MH Phillips, KA Frankel, JI Fabrikant. Stereotactic frame for neuroradiology and charged particle Bragg peak radiosurgery of intracranial disorders. *Int J Radiat Oncol Biol Phys*, 16:1615-1621, 1989.
- [31] LA Melnikov, BA Konnov, NN Yalynych. Radiosurgery of cerebral AVM. In *International Workshop on Proton and Narrow Photon Beam Therapy*, pages 92-98. Oulu, Finland, 1989.
- [32] YeI Minakova. Review of twenty years proton therapy clinical experience in Moscow. In *Proceedings of the Second International Charged Particle Workshop*, pages 1-23. Loma Linda, CA, 1987.
- [33] YeI Minakova. Twenty years clinical experience of narrow proton beam therapy in Moscow. In *Proceedings of the International Heavy Particle Therapy Workshop*. Paul Scherrer Institute, Villigen, Switzerland, 1990.
- [34] YeI Minakova, LL Goldin, VS Khoroshkov, GV Makarova, GD Monzul, KK Onosovski. Proton therapy at ITEP. In *Proceedings of the International Heavy Particle Therapy Workshop*. Paul Scherrer Institute, Villigen, Switzerland, 1990.
- [35] YeI Minakova, LYe Kirpatovskaya, FM Lyass, et al. Proton therapy of pituitary adenomas. *Med Radiol (Mosk)*, 28 (10):7-13, 1983. (in Russian).
- [36] MH Phillips, KA Frankel, JT Lyman, JI Fabrikant, RP Levy. Comparison of different radiation types and irradiation geometries in stereotactic radiosurgery. *Int J Rad Onc Biol Phys*, 18:211-220, 1990.
- [37] MH Phillips, M Kessler, F Chuang, KA Frankel, JI Fabrikant, RP Levy. Correlation of cerebral angiography, computed tomography and magnetic resonance images in the stereotactic charged particle radiosurgical treatment of intracranial arteriovenous malformations. *Int J Rad Onc Bio Phys*, 20: 881-889, 1991.

- [38] MH Phillips, KA Frankel, JT Lyman, JI Fabrikant, RP Levy. Heavy charged-particle stereotactic radiosurgery: Cerebral angiography and CT in the treatment of intracranial vascular malformations. *Int J Radiat Oncol Biol Phys*, 17:419-426, 1989.
- [39] B Sarby. Cerebral radiation surgery with narrow gamma beams. Physical experiments. *Acta Radiol Ther Phys Biol*, 13:425, 1974.
- [40] G K Steinberg, J I Fabrikant, M P Marks, R P Levy, K A Frankel, M H Phillips, L M Shuer, G D Silverberg. Stereotactic heavy-charged-particle Bragg-peak radiation for intracranial arteriovenous malformations. *N Eng J Med*, 323: 96-101, 1990.
- [41] K Stelzer, B Griffin, J Eskridge, J Eenmaa, M Mayberg, S Hummel, H R Winn. Results of neutron radiosurgery for inoperable arteriovenous malformations of the brain. *Medical Dosimetry*, 16: 137-141, 1991.
- [42] K Stelzer, B Griffin, J Eskridge, J Eenmaa, M Mayberg, S Hummel, H R Winn. Neutron radiosurgery for large inoperable arteriovenous malformations of the brain. Submitted to *Neurosurgery*.
- [43] CA Tobias. Pituitary radiation: radiation physics and biology. In JA Linfoot, editor, *Recent Advances in the Diagnosis and Treatment of Pituitary Tumors*, pages 221-243. Raven Press, New York, 1979.
- [44] CA Tobias, HO Anger, JH Lawrence. Radiologic use of high energy deuterons and alpha particles. *American Journal of Roentgenology, Radium Therapy and Nuclear Medicine*, 67:1-27, 1952.
- [45] CA Tobias, JH Lawrence, JL Born, RK McCombs, JE Roberts, HO Anger, BVA Low-Beer, CB Huggins. Pituitary irradiation with high-energy proton beams: a preliminary report. *Cancer Res*, 18:121-134, 1958.

LAWRENCE BERKELEY LABORATORY
UNIVERSITY OF CALIFORNIA
TECHNICAL INFORMATION DEPARTMENT
BERKELEY, CALIFORNIA 94720